Acta Crystallographica Section D
**Biological Crystallography**
ISSN 0907-4449

# The structure of human leucine carboxyl methyltransferase 1 that regulates protein phosphatase PP2A

**Meng-Lin Tsai,[a] Nora Cronin[b] and Snezana Djordjevic[a]***

[a]Institute of Structural and Molecular Biology, Division of Biosciences, University College London, Gower Street, London WC1E 6BT, England, and [b]Institute of Structural and Molecular Biology, Birkbeck College, University of London, Malet Street, London WC1E 7HX, England

Correspondence e-mail: snezana@biochem.ucl.ac.uk

Received 31 May 2010
Accepted 18 October 2010

**PDB Reference:** leucine carboxyl methyltransferase 1, 3o7w.

Leucine carboxyl methyltransferase 1 (LCMT1) methylates the terminal carboxyl group of the leucine 309 residue of human protein phosphatase 2A (PP2A). PP2A, a key regulator of many cellular processes, has recently generated additional interest as a potential cancer-therapeutic target. The status of PP2A methylation impacts upon the selection of the regulatory subunit by the PP2A core enzyme, thus directing its activity and subcellular localization. An X-ray crystal structure of human LCMT1 protein in complex with the cofactor *S*-adenosylmethionine (AdoMet) has been solved to a resolution of 2 Å. The structure enables the postulation of a mode of interaction with protein phosphatase PP2A and provides a platform for further functional studies of the regulation of methylation of PP2A.

## 1. Introduction

Protein phosphatase 2A (PP2A) is an important regulator of many cellular processes, including cell-cycle regulation (Gabel *et al.*, 1999; Karaiskou *et al.*, 1999; Lee, 1995; Perdiguero & Nebreda, 2004; Wang & Ng, 2006), DNA replication (Lin *et al.*, 1998; Yan *et al.*, 2000), mRNA translation (Andjelkovic *et al.*, 1996; Cho *et al.*, 2006), signal transduction (Anderson *et al.*, 1990; Gomez & Cohen, 1991; Lechward *et al.*, 2001; Liauw & Steinberg, 1996; Millward *et al.*, 1999; Zolnierowicz, 2000) and apoptosis (Chatfield & Eastman, 2004; Chen *et al.*, 2006; Chiang *et al.*, 2003; Alvarado-Kristensson & Andersson, 2005; Xin & Deng, 2006). Abnormal activity of PP2A leads to hyperphosphorylation of the tau protein, contributing to the pathology of Alzheimer's disease (Tanimukai *et al.*, 2005; Tian & Wang, 2002; Tsujio *et al.*, 2005). In addition, PP2A has been identified as a tumour suppressor in lung and colon cancer, highlighting this molecule as a potential target for novel cancer-therapeutic strategies (Janssens *et al.*, 2005; Schonthal, 2001; Van Hoof & Goris, 2004).

The core structure of PP2A ($PP2A_D$) is composed of two subunits: a 65 kDa scaffolding subunit A ($PP2A_A$) and a 36 kDa catalytic subunit C ($PP2A_C$). Each subunit has two isoforms, $\alpha$ and $\beta$, which share high sequence similarity (Arino *et al.*, 1988; Hemmings *et al.*, 1990; Stone *et al.*, 1987). The scaffolding subunit A consists of 15 tandem huntingtin-elongation-A subunit-TOR (HEAT) repeats which are organized into a horseshoe shape (Groves *et al.*, 1999). The catalytic subunit C contains an $\alpha/\beta$-fold of the catalytic domain and shares a highly conserved sequence and catalytic mechanism with other serine/threonine phosphatases of the

phosphothreonin phosphatase (PPP) family, such as PP1, PP2B and PP2C (Cho & Xu, 2007; Xu *et al.*, 2006). The core enzyme $PP2A_D$ combines with one of the variable regulatory subunits to form a trimeric complex, $PP2A_T$, also referred to as the holoenzyme. At least 17 of the regulatory subunits can be classified into four distinct functional subfamilies: B (PR55), B′ (PR61), B″ (PR48/PR59/PR72/PR130) and B‴ (PR93/PR110). Sequence similarity and structural conservation among these four subfamilies is very low (Cho & Xu, 2007; Xu *et al.*, 2006, 2008). Combination of the core $PP2A_D$ enzyme with one of the many regulatory B subunits determines substrate specificity, facilitates cellular localization and regulates the enzymatic activity of PP2A (Janssens & Goris, 2001). (Throughout the text the notation PP2A refers to any form of the enzyme where it has not been demonstrated that a particular assembly is required or involved in a given activity or phenomenon.)

PP2A is regulated through two main mechanisms: phosphorylation and methylation. Both modifications occur at the carboxyl-terminal motif (residues 294–309) of $PP2A_C$, which is highly conserved in all other serine/threonine phosphatases. $PP2A_C$ has been shown to be phosphorylated by the epidermal growth factor (EGF) and insulin receptors and by other tyrosine kinases including the leukocyte-specific protein tyrosine kinase (LCK) and the viral sarcoma (v-SRC) kinase (Chen *et al.*, 1992). Phosphorylation of the C-terminal tail of $PP2A_C$ at Tyr307 results in the inactivation of PP2A (Begum & Ragolia, 1996, 1999; Chen *et al.*, 1994; Srinivasan & Begum, 1994). However, methylation of the terminal carboxylate group of the Leu309 residue of $PP2A_C$ by the specific protein methyltransferase has been postulated to lead to enzyme activation (Favre *et al.*, 1994; Lee & Stock, 1993; Xie & Clarke, 1993). Leucine carboxyl methyltransferase 1 (LCMT1) and protein phosphatase methylesterase 1 (PME1) have been identified as the major mammalian methyltransferase and methylesterase of PP2A (De Baere *et al.*, 1999; Ogris *et al.*, 1999). However, at least two studies have shown that $PP2A_C$ methylation is either unrelated to PP2A activity or leads to a decrease in activity (De Baere *et al.*, 1999; Zhu *et al.*, 1997), suggesting that $PP2A_C$ methylation may be linked to other aspects of PP2A function.

The precise structural role and cellular function of the reversible modification of PP2A is still a subject of debate. While it has been demonstrated that methylation of Leu309 was necessary for $PP2A_D$ association with the regulatory subunit PR55 *in vitro* (Bryant *et al.*, 1999) and that $PP2A_T$ was fully methylated when it recruited the B″ (PR72) or B‴ subunits *in vivo*, $PP2A_C$ of the holoenzyme purified from porcine brain was not fully methylated when in association with the PR55 B subunit (De Baere *et al.*, 1999). Furthermore, the loss of carboxyl methyltransferase activity decreased but did not abrogate the formation of $PP2A_T$ with the PR55 regulatory subunit (Guo *et al.*, 2002; Wu *et al.*, 2000). Recently, another molecule has been identified as a regulator of PP2A activity: protein phosphatase 2A activator (PTPA), a peptidyl-prolyl *cis*/*trans*-isomerase. *In vitro* experiments have shown that the catalytically inactive $PP2A_C$ forms a complex with PME1 that can only be reactivated by PTPA, but not by methyltransferase activity alone (Jordens *et al.*, 2006; Longin *et al.*, 2004).

In 2006, the crystal structure of the PP2A holoenzyme was determined by two research groups (Cho & Xu, 2007; Xu *et al.*, 2006). Based on the three-dimensional structure of PP2A, the methylation of the C-terminal tail of subunit C at Leu309 was predicted to neutralize the negatively charged surface present at the AC interface and thus recruit subunit B′ (PR61) to form a stable holoenzyme (Cho & Xu, 2007; Xu *et al.*, 2006). It was proposed that through this mechanism methylation assists in the assembly of the PP2A holoenzyme and that methylation is required for the recruitment of the B′ subunit (PR61). In contrast, recent data suggest that methylation of PP2A subunit C is not absolutely required for the binding of the B′ (PR61) or B″ (PR72) families but is required for the binding of the B (PR55) family *in vivo* (Longin *et al.*, 2007). Although it is very clear that the methylation state is a key factor in the assembly of a PP2A holoenzyme, the discrepancies in the literature with respect to the relationship between the methylation state and the type of regulatory subunit (B, B′ or B‴) within the heterotrimeric complex emphasize the need for further investigation of this phenomenon.

Additional interest in PP2A methylation stems from the suggested link between the deregulation of PP2A methylation and the pathology of Alzheimer's disease. The activity of LCMT1 is AdoMet-dependent and is inhibited by *S*-adenosylhomocysteine (SAH). Elevated SAH levels in the blood lead to a decrease in PP2A methylation and might be related to down-regulation of PP2A and the accumulation of phosphorylated tau protein (Sontag *et al.*, 2007; Zhang *et al.*, 2008).

Previously, we have reported the crystallization of human LCMT1; however, the crystals were of poor diffraction quality (George *et al.*, 2002). Based on limited proteolysis experiments and sequence homology to the *Saccharomyces cerevisiae* homologue protein phosphatase methyltransferase 1 (PPM1; Leulliot *et al.*, 2004), we have generated a new expression construct and successfully crystallized the protein. Here, we report the X-ray crystal structure of human leucine carboxyl methyltransferase 1 in complex with the cofactor *S*-adenosylmethionine. We compare human LCMT1 with the *S. cerevisiae* PPM1 protein and propose a putative mode of interaction of LCMT1 with its substrate PP2A.

## 2. Materials and methods

### 2.1. The limited-proteolysis method and expression-construct design

For the limited-proteolysis experiments, 1 µg trypsin was added to 1 mg freshly purified full-length LCMT1. The reaction mixture was incubated at room temperature and aliquots were removed for SDS–PAGE analysis after 10, 30 and 60 min and subsequently at hourly intervals until the reaction had ended. After protease digestion, the sample was immobilized on a PVDF membrane (GE Healthcare) *via* transfer buffer

(10 m*M* CAPS pH 11.0, 10% methanol) with a constant voltage of 250 mA for 2 h and the target band on the membrane, stained using CBB stain (0.025% Coomassie Blue R-250, 40% methanol), was sent to the Protein and Nucleic Acid Chemistry Facility (PNAC) at Cambridge University for N-terminal protein-sequence analysis. For determination of the molecular weight of a target segment or domain, a 1 mg ml$^{-1}$ protein sample in 10 m*M* ammonium acetate buffer pH 6.4 was analyzed at the Mass Spectrometry Facility at the Institute of Structural and Molecular Biology at UCL.

The DNA sequence for LCMT1$_{SD20–334}$ was amplified by polymerase chain reaction (PCR) using cDNA of the human full-length LCMT1 as a template. A nested PCR protocol with two pairs of primers was used to generate the construct. One pair of primers generated a DNA product coding for residues 20–232 followed by an EG linker and then residues 259–262 (KSLE) of LCMT1$_{SD20–334}$; a *Pci*I restriction site was introduced at the 5′ end of the PCR fragments, while the reverse primer (5′-CTGTGACTCTAATGATTTGCCTTCGTTCAC-CTGTTCGTA-3′) corresponded to the complementary DNA strand of the amino-acid sequence YEQVN-EG-KSLE, where the YEQVN sequence comprises residues 228–232 of LCMT1. The second pair of primers consisted of a forward primer (5′-TACGAACAGGTGAACGAAGGCAAATCATTAGAGTC-ACAG-3′) coding for the YEQVN-EG-KSLE amino-acid sequence and a reverse primer that introduced a *Hin*dIII restriction site and a stop codon at the 3′ end of the fragment. Combination of the two fragments yielded a PCR amplicon encoding residues 20–232 linked through the EG dipeptide to residues 259–334 of human LCMT1.

### 2.2. Protein expression and purification

Truncated methyltransferase LCMT1$_{SD20–334}$ was cloned into a pET30a vector (Novagen) containing an N-terminal polyhistidine affinity tag and a tobacco etch virus (TEV) protease cleavage site to allow removal of the affinity tag. The expression construct was verified by DNA sequencing (Eurofin-MWG). LCMT1$_{SD20–334}$ was overexpressed in *Escherichia coli* BL21 (DE3) pLysS cells. Protein expression was induced by the addition of 0.5 m*M* IPTG and the culture was allowed to grow for a further 5 h while shaking at 303 K. The cells were then harvested by centrifugation and the pellets were stored at 253 K until required. The cell pellets were defrosted, resuspended in sonication buffer consisting of 50 m*M* Tris–HCl pH 8.0, 50 m*M* NaCl, 2 m*M* $\beta$-mercaptoethanol and Complete EDTA-free protease-inhibitor cocktail (Roche) and lysed by sonication. The lysate was centrifuged at 13 000*g* for 1 h. The supernatant was applied onto an Ni–NTA column (Qiagen) and the protein was purified following the manufacturer's instructions. The eluted proteins were dialyzed overnight in a sonication buffer at 277 K in the presence of TEV protease. The protease and the cleaved polyhistidine tag were removed by passing the dialyzed material over an Ni–NTA column, while LCMT1 protein was collected in a flow-through fraction. In a final purification step, the flowthrough fraction containing LCMT1 was subjected to size-exclusion chromatography on a Superdex 200 column (GE Healthcare).

PP2A$_A$ was expressed and purified as described previously (Groves *et al.*, 1999) except that a Superdex 200 size-exclusion column was used instead of Superose 200. In addition, 40% ammonium sulfate was used to precipitate small traces of a contaminant protein following size-exclusion chromatography. The precipitate was separated by centrifugation and the supernatant was dialyzed in a buffer consisting of 25 m*M* Tris–HCl pH 8.0, 50 m*M* NaCl and 1 m*M* $\beta$-mercaptoethanol.

**Table 1**
Data-collection and refinement statistics for LCMT1$_{SD20–334}$.

Values in parentheses are for the outer shell.

| | |
|---|---|
| Crystal data | |
| Space group | $P2_12_12_1$ |
| Unit-cell parameters (Å) | $a$ = 49.1, $b$ = 63.3, $c$ = 81.8 |
| Resolution (Å) | 17.53–2.00 (2.07–2.00) |
| Measured reflections | 76195 (4418) |
| Unique reflections | 17062 (1587) |
| Completeness (%) | 96.0 (91.2) |
| $R_{merge}$† | 0.057 (0.335) |
| $\langle I/\sigma(I)\rangle$ | 17.5 (2.2) |
| Refinement statistics | |
| Resolution range | 17.53–2.00 (2.07–2.00) |
| $R_{cryst}$ | 0.20 |
| $R_{free}$ | 0.26 |
| Mean $B$ factor (Å$^2$) | 32.8 |
| Water molecules | 138 |
| R.m.s. deviations from ideal‡ | |
| Bond lengths (Å) | 0.016 |
| Bond angles (°) | 1.6 |
| Ramachandran plot (%) | |
| Residues in favoured region | 98.6 |
| Residues in allowed region | 100 |

† $R_{merge} = \sum_{hkl}\sum_i |I_i(hkl) - \langle I(hkl)\rangle| / \sum_{hkl}\sum_i I_i(hkl)$, where $I_i(hkl)$ is the $i$th used observation for unique $hkl$ and $\langle I(hkl)\rangle$ is the mean intensity for unique $hkl$. ‡ With respect to Engh and Huber parameters (Engh & Huber, 1991).

### 2.3. High-throughput screening of crystallization conditions

Following large-scale purification, variant LCMT1 proteins were concentrated to at least 10 mg ml$^{-1}$ (30 mg ml$^{-1}$ in the case of LCMT1$_{SD20–334}$), a 1.2-fold molar excess of AdoMet was added to the protein solution and the samples were subjected to crystallization trials using the sitting-drop vapour-diffusion method with commercial screening suites including Index (Hampton Research), PGA Screen (Molecular Dimensions), PEGs Suite (Qiagen), JBScreen PEG/Salt (Jena Bioscience), JCSG (Qiagen), JBScreen Classic II (Jena Bioscience) and NeXtal Cryo Suite (Qiagen). A Mosquito robot (TTP LabTech), which provides accurate sample placement for drop dispensing, was used for automated high-throughput crystallization screening, with the sitting drops prepared by mixing 0.1 µl protein solution and 0.1 or 0.2 µl reservoir solution in a 96-well plate format (Qiagen). All crystallization trays were incubated at 293 K. LCMT1$_{SD20–334}$ was the only protein variant that crystallized within several days under the range of conditions, which included diverse precipitants.

### 2.4. X-ray diffraction and data collection

The crystal that was used to obtain the X-ray diffraction data was grown from a solution containing pentaerythritol ethoxylate and the crystal was flash-frozen directly in a cold nitrogen stream. The X-ray diffraction data were collected on a 300 mm Saturn 944+ CCD detector using an AFC-11 four-axis partial $\chi$ goniometer with a Rigaku MicroMax-007 HF rotating-anode X-ray generator equipped with Varimax VHF optics. 180° of data were collected over 0.5° oscillations and the diffraction images were scaled and the data were merged and indexed using the program *d*TREK* (Pflugrath, 1999). The crystals belonged to space group $P2_12_12_1$, with unit-cell parameters $a = 49.09$, $b = 63.30$, $c = 81.77$ Å, $\alpha = \beta = \gamma = 90°$ and one molecule of LCMT1 per asymmetric unit. The unit-cell parameters and data-collection statistics are listed in Table 1.

### 2.5. Structure determination and refinement

The structure of human LCMT1 was determined by the molecular-replacement method using the programs *Phaser* and *MOLREP* from the *CCP*4 suite v.6.1.3 (McCoy *et al.*, 2007; Vagin & Teplyakov, 2010; Collaborative Computational Project, Number 4, 1994) and a homology model for the core structure of LCMT1 that was based on the coordinates of *S. cerevisiae* protein phosphatase methyltransferase 1 (PDB entry 1rjg; Leulliot *et al.*, 2004) as the starting model. The initial model covered ∼75% of the amino-acid residues present in the polypeptide chain used to obtain the crystals. Electron density for the cofactor, which was not included in the molecular-replacement model, was clearly visible in the initial maps, providing confirmation of the molecular-replacement solution. Structure refinement was carried out using the maximum-likelihood restrained method with simple scaling in *REFMAC*5 from *CCP*4 (Murshudov *et al.*, 1997) as well as the solvent-flattening and density-modification routines implemented in *CCP*4. Real-space refinement/manual fitting of the electron-density map and model building were carried out in *Coot* v.0.6.1 (Emsley *et al.*, 2010). The final model of LCMT1 includes residues 29–232, the EG dipeptide linker and residues 259–334. In addition, a single molecule of AdoMet and a glycerol molecule were included in the model. The model was validated using *Coot*, *PROCHECK* (Laskowski *et al.*, 1993) and *MolProbity* (Chen *et al.*, 2010). No Ramachandran outliers were detected and the model generated a good *MolProbity* score of 2.1 with H atoms added prior to the analysis. *MolProbity* was very valuable in identifying a significant number of poor rotamers, in particular those of Leu residues, which were subsequently corrected such that the final model contained only 4% of poor rotamers, many of which were constrained by intramolecular interactions with other residues in the structure. While the core of the structure fitted well into the electron density, there were regions that exhibited a high level of disorder, in particular a large loop region (residues 303–313) and the C-terminal end (residues 325–334). The atomic coordinates for the LCMT1 structure have been deposited in the Protein Data Bank (http://www.pdb.org; Berman *et al.*, 2000) with code 3o7w.

### 2.6. Isothermal titration calorimetry

Isothermal titration calorimetry experiments were carried out in a reaction buffer consisting of 50 m*M* Tris pH 8.0, 50 m*M* NaCl, 1 m*M* DTT using a VP-ITC titration calorimeter (MicroCal) with a reaction-cell volume of 1.4 ml at 286 K. Before running binding experiments, full-length LCMT1 and $PP2A_A$ samples were each dialyzed in the same buffer and all solutions, including the buffer that was used for heat dilution measurements, were degassed and filtered just before loading into the calorimeter. 10 µ*M* $PP2A_A$ in the reaction cell was titrated with a stock solution of 100 µ*M* native LCMT1. 19 consecutive LCMT1 injections of 15 µl at 2 s µl$^{-1}$ were applied at 4 min intervals while stirring the reaction solution at a constant speed of 300 rev min$^{-1}$. For heat dilution of the protein, 1.4 ml reaction buffer in the reaction cell was titrated with 300 µl 100 µ*M* full-length LCMT1 and this value was subtracted from the measured heats of binding. The protein concentrations of the samples used in these experiments were estimated by UV absorbance measurements at 280 nm, with a calculated extinction coefficient of 42 400 $M^{-1}$ cm$^{-1}$ for $LCMT1_{SD20–334}$ and $PP2A_A$, as they both contain the same numbers of tyrosine and tryptophan residues.

## 3. Results and discussion

### 3.1. Protein engineering of human leucine carboxyl methyltransferase 1 and protein crystallization

Although full-length human LCMT1 can be expressed in and purified from *E. coli* (George *et al.*, 2002), no crystals were obtained of this form of the protein and further expression gene constructs for LCMT1 were designed. PPM1 from *S. cerevisiae* shares ∼29% sequence identity with human LCMT1. Amino-acid sequence alignment with *S. cerevisiae* PPM1 using *ClustalW* v.1.83 (Larkin *et al.*, 2007), together with a comparison of the human LCMT1 secondary-structure prediction obtained by *PSIPRED* (Bryson *et al.*, 2005) and the secondary structure from the crystal structure of yeast PPM1 (Leulliot *et al.*, 2004), suggested secondary-structure conservation beginning from residue Asp20 of LCMT1. Therefore, several residues preceding the first predicted $\alpha$-helix of LCMT1, including Arg6, Glu7, Ser9, Thr16 and Asp20, were chosen as potential starting N-terminal residues of the protein products, while the residues following the last predicted $\beta$-strand of LCMT1 (Thr321 and Aspr329) were selected as alternative C-termini of the protein products to be generated for crystallization studies. Fig. 1 shows a summary of the protein products generated and their solubility properties; the superscripts denote the starting and ending residues in the full-length LCMT1 sequence. Truncation at residue Thr321 at the C-terminus of LCMT1 rendered the resulting proteins insoluble. The yields of soluble protein generated from the other expression constructs were relatively low and their levels were enhanced through co-expression with chaperonins (GroES/GroEL; George *et al.*, 2002). $LCMT1_{20–334}$ was the only protein product that was crystallized in a complex with the cofactor *S*-adenosylmethionine, from the optimized crys-

tallization conditions 0.1 *M* sodium citrate pH 6.5, 1.6 *M* ammonium sulfate, 0.38 *M* sodium/potassium tartrate, 2% PEG 400, 4% acetone and 5 m*M* DTT at 295 K. However, these crystals only diffracted to 7 Å resolution and were not suitable for structure determination. Several methods were used to improve the diffraction quality of the crystals, including the additive-screening method (Hampton Research), dehydration using MicroRT Capillaries (MiTeGen) and the crystal-annealing and seeding method (Hampton Research), but no method was successful in increasing the diffraction resolution, suggesting that additional protein constructs would need to be considered for crystallization in order to obtain a different crystal form.

Limited proteolysis has been used successfully by many laboratories to probe conformational features of proteins and to identify the most stable fragments or domains in protein structures (Fontana *et al.*, 2004). SDS–PAGE analysis showed that limited proteolysis of LCMT1 resulted in a single stable polypeptide band with migration properties corresponding to a molecular weight of approximately 27 kDa. The protein-sequence result showed that the first six residues at the N-terminus were $E^{7}SSITS^{12}$, while the molecular weight of this proteolytic product was 26.8 kDa, as verified by mass spectrometry. These two analyses and prediction of trypsin-digestion sites of LCMT1 suggested that the C-terminal residue of the main proteolytic product could be Arg236. Arg236 of human LCMT1 corresponds to residue Arg242 in the previously reported flexible region of the *S. cerevisiae* PPM1 structure (Leulliot *et al.*, 2004). The combination of the prediction of LCMT1 secondary structure, together with the amino-acid sequence comparison to yeast PPM1, led us to propose that the region between residues Asn232 and Lys259 in human LCMT1 may also be highly flexible and might interfere with crystallization. Therefore, three LCMT1 constructs were designed: $LCMT1_{7–334}$ containing residues 7–232, a small linker EG and residues 259–334, an $LCMT1_{7–232}$ construct including residues 7–232 only and an $LCMT1_{SD20–334}$ construct including residues 20–232, a small linker EG and residues 259–334. A similar strategy involving excision of the flexible region has previously been employed to generate a suitable protein for crystallization of the human PP2A methylesterase (Xing *et al.*, 2008). Perhaps not surprisingly, $LCMT1_{7–232}$ failed to yield soluble protein. In contrast, both protein products lacking a putative flexible region were soluble and the levels of soluble protein expression were significantly higher than previously obtained, such that we were able to purify about 8 mg of protein per litre of cells in the absence of any chaperonins. In the initial screen of 700 crystallization conditions with the $LCMT1_{SD20–334}$ protein, about 100 conditions produced crystals. The successful crystallization conditions contained a range of different precipitants, including PEG 3350, PEG 5000, PEG 8000, ammonium sulfate or Jeffamine ED-2001. A single crystal from one of the conditions (0.05 ammonium sulfate, 0.05 *M* bis-tris chloride pH 6.5, 30% pentaerythritol ethoxylate) was used to collect the diffraction data that were used to solve the structure.

| Construct | Amino-acid sequence | Solubility | Crystallization |
|---|---|---|---|
| $LCMT1_{1–334}$ | N1 → 334C | + | – |
| $LCMT1_{6–334}$ | N6 → 334C | + | – |
| $LCMT1_{1–329}$ | N1 → 329C | + | – |
| $LCMT1_{6–329}$ | N6 → 329C | + | – |
| $LCMT1_{24–329}$ | N24 → 329C | + | – |
| $LCMT1_{26–329}$ | N26 → 329C | – | – |
| $LCMT1_{7–321}$ | N7 → 321C | – | – |
| $LCMT1_{9–321}$ | N9 → 321C | – | – |
| $LCMT1_{20–321}$ | N20 → 321C | – | – |
| $LCMT1_{20–334}$ | N20 → 334C | + | + |
| $LCMT1_{61–334}$ | N61 → 334C | + (soluble aggregates) | – |
| $LCMT1_{7–232}$ | N7 → 232C | – | – |
| $LCMT1_{7–334}$ | N7 → $^{232}$EG$^{259}$ → 334C | + | – |
| $LCMT1_{SD20–334}$ | N20 → $^{232}$EG$^{259}$ → 334C | + | + |

**Figure 1**
A schematic summary of the protein constructs used in this study. Polypeptide chains are represented by arrows, with the N-terminal and the C-terminal residues indicated. The lengths of the arrows are roughly proportional to the number of amino acids in order to emphasize the differences between the protein products.

### 3.2. The overall structure of human leucine carboxyl methyltransferase 1

Human LCMT1 belongs to the class I AdoMet-dependent MTase family, which is a member of the FAD/NAD(P)-binding Rossmann-fold superfamily (Fig. 2*a*; Schubert *et al.*, 2003). The main structural feature of LCMT1 is a seven-stranded $\beta$-sheet flanked by $\alpha$-helices, with the core $\beta$-strands arranged in the following order: $\beta3$, $\beta2$, $\beta1$, $\beta4$, $\beta5$, $\beta7$ and $\beta6$. The strands ($\beta1$–$\beta5$ and $\beta6$) surrounded by the six $\alpha$-helices ($\alpha$Z and $\alpha$A–$\alpha$E) are parallel, whereas $\beta7$ is antiparallel (Fig. 2*a*). In addition to the core domain, several insertions were observed in the human LCMT1 structure. Structural insertions in members of the Rossmann-fold superfamily contain substrate-recognition motifs and variations in these insertions amongst the methyltransferases are associated with observed differences in their substrate specificities (Martin & McMillan, 2002).

Even orthologous proteins from different species exhibit significant differences in these embellishments to the core protein fold. Based on the spatial arrangement around the central $\beta$-sheet in human LCMT1, variations in the core topology can be grouped into three regions: the $\beta3$–$\beta2$ region, the $\beta1$–$\beta4$–$\beta5$ region and the $\beta7$–$\beta6$ region. In the $\beta3$–$\beta2$ region helix $\alpha3$ and strand $\beta$A join helix $\alpha$B to $\alpha$C to pack against strands $\beta3$ and $\beta2$. Although other proteins might have embellishments at this site, their structures differ significantly. For example, in the structure of the bacterial protein methyltransferase CheR there is a small $\beta$ subdomain at this position which serves as a point of attachment to its membrane-associated substrate (Djordjevic & Stock, 1997). In the $\beta1$–$\beta4$–$\beta5$ region, helices $\alpha4$, $\alpha1$ and $\alpha2$ are placed at the C-terminal edge of the central $\beta$-sheet, near the entrance to the enzyme active site. The location of the N-terminal helices $\alpha1$ and $\alpha2$ is similar to the location of the N-terminal regions in other methyltransferases in which they have been implicated in substrate recognition (Djordjevic & Stock, 1997). In the $\beta7$–$\beta6$ region, three helices, $\alpha5$, $\alpha6$ and $\alpha7$, create a topological insertion arranged in a triangular fashion while packing against helix $\alpha$Z through hydrophobic interactions. Helices $\alpha1$, $\alpha5$, $\alpha6$ and $\alpha7$, as well as the associated connecting loops, are all in the vicinity of helix $\alpha$Z such that they completely bury the N-terminal end of helix $\alpha$Z inside the hydrophobic core of the protein (Fig. 2*b*). The role of the described topological

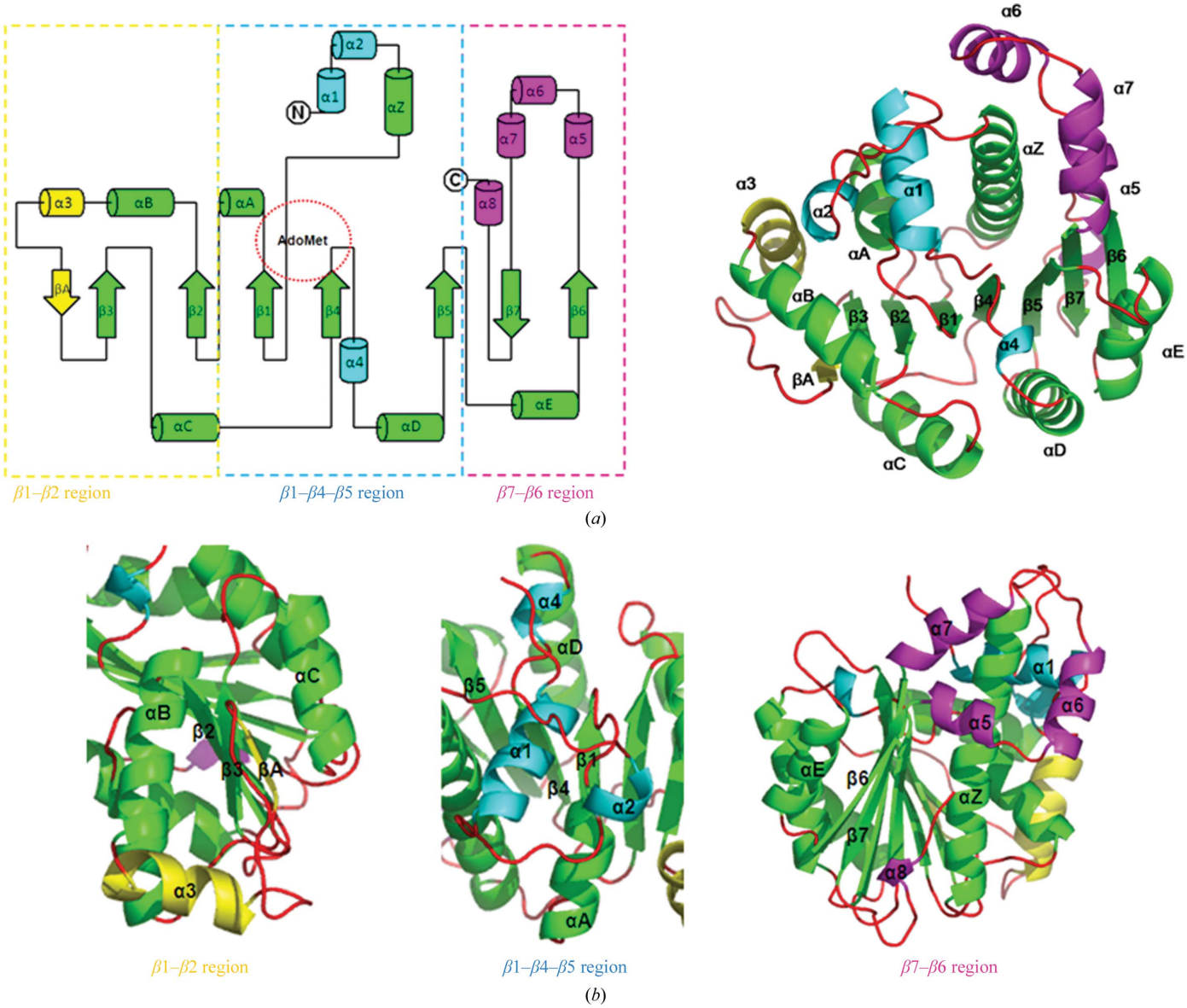


**Figure 2**
The structure of LCMT1. (*a*) Left: topology diagram of human leucine carboxyl methyltransferase 1. The core structure of LCMT1 consisting of a seven-stranded $\beta$-sheet ($\beta3$, $\beta2$, $\beta1$, $\beta4$, $\beta5$, $\beta7$ and $\beta6$) flanked by six $\alpha$-helices ($\alpha$Z and $\alpha$A–$\alpha$E) belongs to the class I AdoMet-dependent methyltransferase 1 family. The secondary-structure elements are represented as follows: the core structure of the methyltransferase, green; insertions in the $\beta3$–$\beta2$ region, yellow; the insertion in the $\beta1$–$\beta4$–$\beta5$ region, cyan; the insertion in the $\beta7$–$\beta6$ region, pink. Right: a ribbon diagram of LCMT1 generated with the *PyMOL* viewer (DeLano Scientific). The same colour scheme was used as in Fig. 1(*a*). (*b*) Detailed view of the structural embellishments to the core methyltransferase domain in regions $\beta3$–$\beta2$ ($\alpha3$ and $\beta$A), $\beta1$–$\beta4$–$\beta5$ ($\alpha1$, $\alpha2$ and $\alpha4$) and $\beta7$–$\beta6$ ($\alpha5$, $\alpha6$, $\alpha7$ and $\alpha8$).

additions and insertions to the Rossmann fold is dual: it is both structural, providing a stabilizing hydrophobic environment for the central $\beta$-sheet, and functional, creating a platform for the site of the specific interactions with the substrate, in this case the PP2A molecule. The crystal structure of human LCMT1 is lacking a 26-residue polypeptide fragment that would represent the fourth site of the topological insertions located between strand $\beta5$ and helix $\alpha$E and this part of the structure would also be placed at the C-terminal edge of the central $\beta$-sheet, thus forming the entrance to the active site together with the other described inserted structural elements (Fig. 3). The corresponding region in the yeast structure, labelled $\alpha$Y in Fig. 3, exhibits great flexibility and it is tempting to postulate that this domain acts as a lid for the active site that enables substrate interaction and that might become ordered upon binding of PP2A. Superimposition of the PPM1 structure including this region and the structure of LCMT1 indicates that the region could not be accommodated within the same crystal form of LCMT1 as it would interfere with crystal packing, which might explain the difficulty in crystallizing the full-length form of the protein.

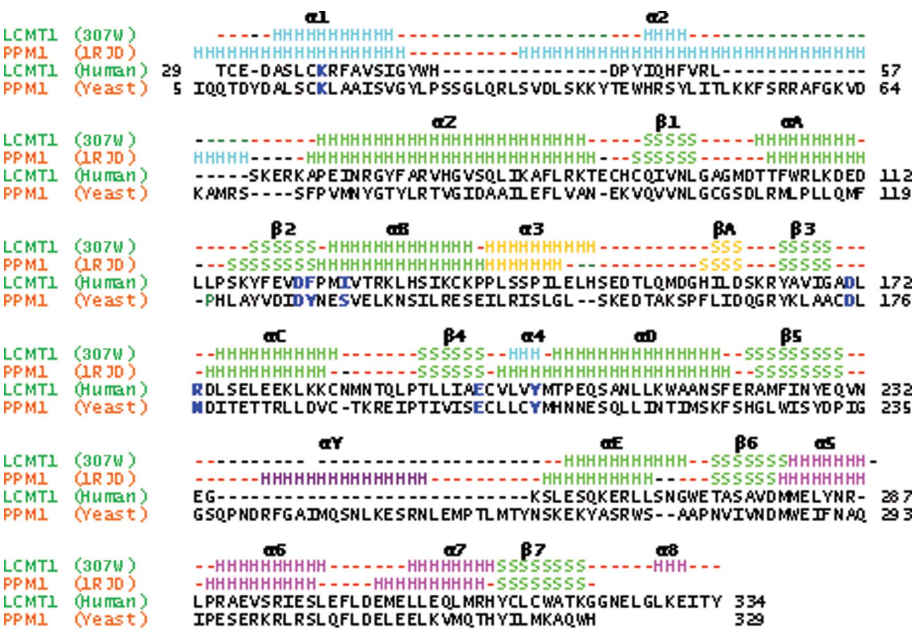


(*a*)

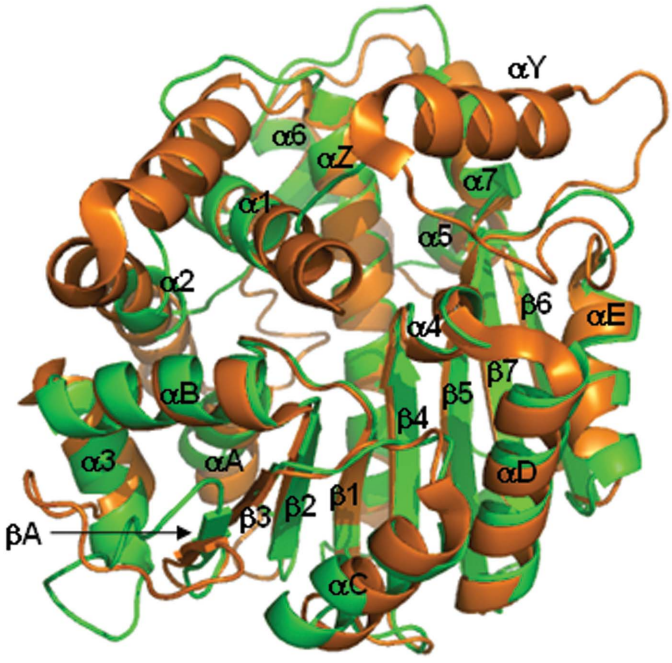


(*b*)

**Figure 3**
Comparison between the LCMT1 and PPM1 structures. The sequence alignment, based on superimposition of the yeast PPM1 and human LCMT1 structures, is shown in (*a*). The secondary-structure elements of human LCMT1 and yeast PPM1 are indicated above the aligned sequences. The colour assignment for the secondary structure of human LCMT1 is the same as in Fig. 1. Dashed lines coloured black and red represent gaps in the sequence alignment and protein loops, respectively. The amino-acid residues coloured blue are associated with AdoMet. (*b*) The *S. cerevisiae* PPM1 (PDB code 1rjg; orange) and human LCMT1 (green) structures were superimposed using *Coot* v.0.6.1. Helix $\alpha$Y in the yeast PPM1 structure is absent from the LCMT1 structure and was replaced by the EG dipeptide.

### 3.3. Comparison of human LCMT1 with *S. cerevisiae* PPM1

The molecular-replacement method was utilized to solve the crystal structure of human LCMT1, using the crystal structure of yeast PPM1 (PDB code 1rjg; Leulliot *et al.*, 2004) to generate a starting model for the rotation/translation-function searches. Initial attempts to solve the structure with a PPM1-based homology model of LCMT1 failed and a successful solution was only obtained with a greatly stripped model of LCMT1. Specifically, the successful molecular-replacement model contained the core structure corresponding to residues 61–321 with all loop/insertion regions removed. The omitted residues were subsequently built into the electron-density maps during the process of model building and refinement. Superimposition of the structures of human LCMT1 and *S. cerevisiae* PPM1 (PDB code 1rjg) using the program *Coot* v.0.6.1 (Emsley *et al.*, 2010) shows that the core regions of the two proteins are very similar, with a root-mean-square distance of 1.3 Å for 231 $C^{\alpha}$ atoms of the aligned residues, despite a relatively low sequence identity for the overlapping sequence (~30%; Fig. 3). As expected, the structures exhibit their main differences

within the associated variable segment. For example, in the $\beta1$–$\beta4$–$\beta5$ region of the human LCMT1 core structure the short helix $\alpha2$ is flanked by two flexible long loops, whereas in the same area of yeast PPM1 this part is replaced by a long $\alpha$-helix with a sharp kink in the middle, giving the appearance of two helices (Fig. 3). In contrast, helix $\alpha1$ within this insertion is strongly conserved in its topology and sequence between LCMT1 and PPM1, most likely as a consequence of the direct participation of this helix in the formation of the AdoMet binding site. Additional variations include conformational differences of the $\alpha3$–loop–$\beta$A connection between helix $\alpha$B and strand $\beta3$, significant differences in the lengths and relative orientations of the C-terminal helices $\alpha5$, $\alpha6$ and $\alpha7$, and the presence of an additional single-helical turn $\alpha8$ at the C-terminal end of LCMT1 (Fig. 3). Clearly, the structural differences reflect species-specific determinants of protein–protein interactions with the respective partner substrates or potential regulatory proteins.

### 3.4. *S*-Adenosylmethionine binding site

An initial electron-density map following the successful molecular-replacement solution was examined for any unmodelled electron density within the core of the LCMT1 structure and we could clearly identify the position and conformation of the AdoMet molecule that was included in the crystallization (Fig. 4*a*). The cofactor adopts an extended conformation that is commonly found in AdoMet-dependent methyltransferases and superimposition of the AdoMet binding sites of human LCMT1 and yeast PPM1 showed that the residues interacting with AdoMet are highly conserved in the two proteins (Fig. 4*b*). The adenine ring of the bound AdoMet is sandwiched between the hydrophobic residues Phe123 and Leu172 in LCMT1, while the equivalent residues in the PPM1 structure are Tyr129 and Leu176, respectively. Similarly, as is the case in many other nucleotide-binding proteins, hydroxyl O atoms from the ribose moiety are positioned in the active site through interaction with the acidic residue Asp122 in LCMT1. At the other end of the AdoMet molecule, the carboxylate group is engaged in an ionic interaction with the conserved residues Lys37 ($\alpha1$) and Arg73 ($\alpha$Z), while the amino group forms hydrogen bonds to the backbone carbonyl O atom of Gly98 ($\beta1$–$\alpha$A connection) and Glu198 ($\beta4$) (Fig. 4*b*). However, further away from the zone of direct interaction with AdoMet, but lining the cavity that creates the binding pocket for the cofactor, there are some

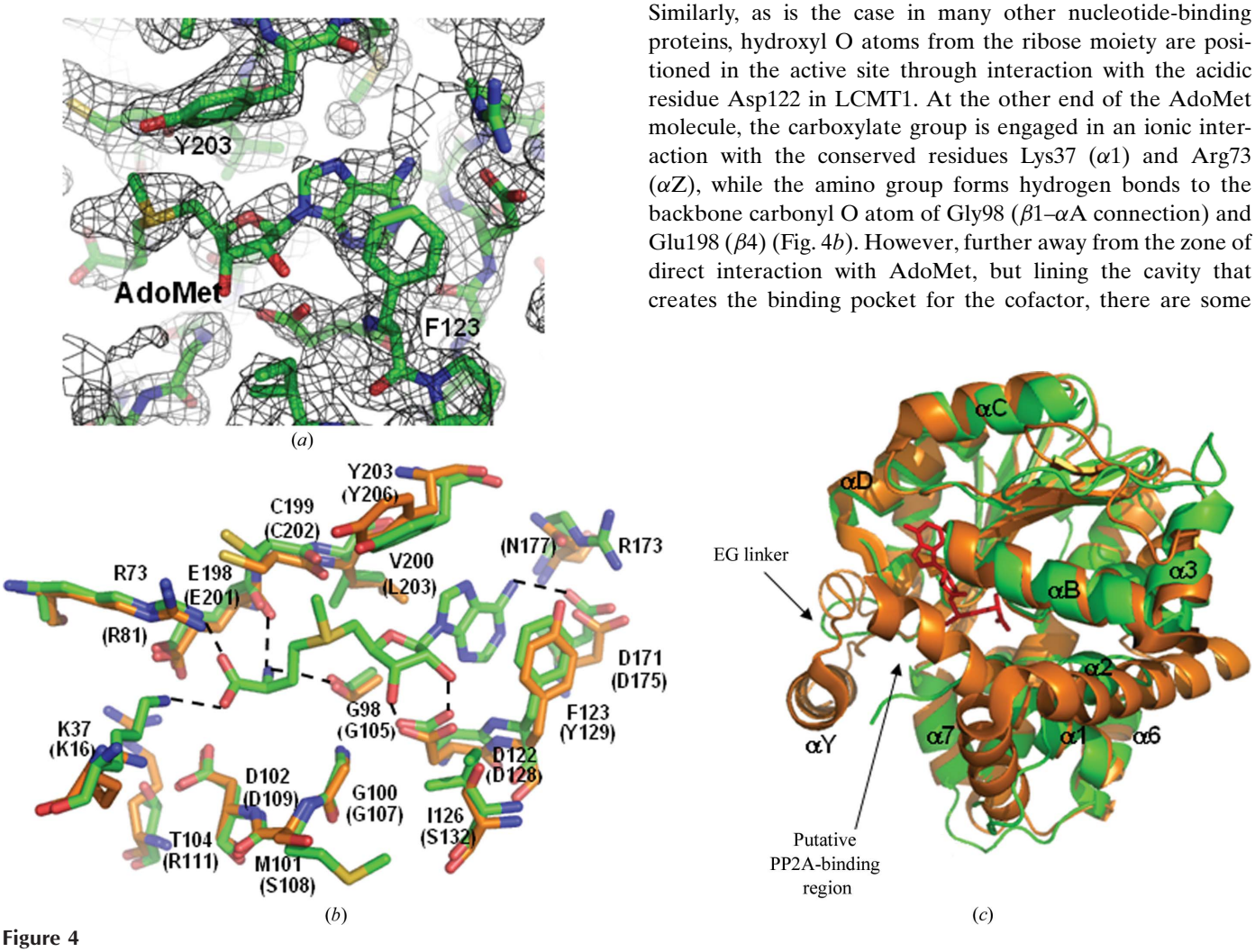


**Figure 4**
Active site of human LCMT1. (*a*) The electron density of AdoMet can clearly be observed in the $\sigma$-weighted ($2mF_o - DF_c$, $\alpha_c$) electron-density map calculated with the initial model after the molecular-replacement solution was obtained. At this stage, the model included only 75% of the residues and no AdoMet. The map is shown at a level of 1.0$\sigma$ (0.33 e Å$^{-3}$) with the final refined coordinates for LCMT1 overlaid. (*b*) Superimposition of the human LCMT1 (green) and yeast PPM1 (orange) structures shows conservation of the AdoMet binding site. Several hydrogen bonds between AdoMet and human LCMT1 residues are indicated as dashed lines. Residue numbers corresponding to PPM1 are shown in parentheses. (*c*) The putative PP2A binding site is indicated on the superimposed structures of human LCMT1 and yeast PPM1. The site of the excision of residues 232–259 and replacement by the EG linker in human LCMT1 is also indicated.

significant differences, such as the presence of Ile126 in LCMT1 in place of Ser132 in PPM1, of Val200 in LCMT1 instead of Leu203 in PPM1 and of Arg173 at the top of the adenine ring in LCMT1 compared with Asn177 at the equivalent position in PPM1.

In the structure of human LCMT1 presented here, AdoMet does not appear to be fully buried in the active site, with the side of the cofactor containing the activated methyl group being relatively exposed; AdoMet has a contact area of 17 Å$^2$ as calculated using *AREAIMOL* from *CCP*4 (Collaborative Computational Project, Number 4, 1994). In contrast, in the structure of yeast PPM1 (PDB code 1rjd) AdoMet is covered by the beginning of the N-terminal helix $\alpha$1, which is partially unravelled in the structure of LCMT1. Although the full-length LCMT1 protein contains an additional 20 residues at the N-terminus, the sequence of this N-terminal segment, which is dominated by Ser and Cys residues, would suggest that this region is unstructured, at least in the absence of substrate, and thus we do not anticipate that the N-terminal residues would occlude AdoMet in the context of the full-length protein. The partially exposed AdoMet and the surrounding funnel-shaped opening indicate an entry site for the carboxyl-terminal motif of the PP2A catalytic subunit ($T^{304}PDYFL^{309}$), which is methylated by LCMT1 on the terminal carboxyl group to form an $\alpha$-leucine ester modification (Fig. 4*c*). Examination of the molecular surface of PPM1 identifies a deep and narrow groove that leads towards the only exposed side of the cofactor: an activated methyl group of the bound AdoMet molecule (Fig. 5*a*). The equivalent orientation of the human LCMT1 molecular surface reveals a similar groove, strongly suggesting that an extended form of the PP2A$_C$ C-terminus might approach AdoMet through this site.

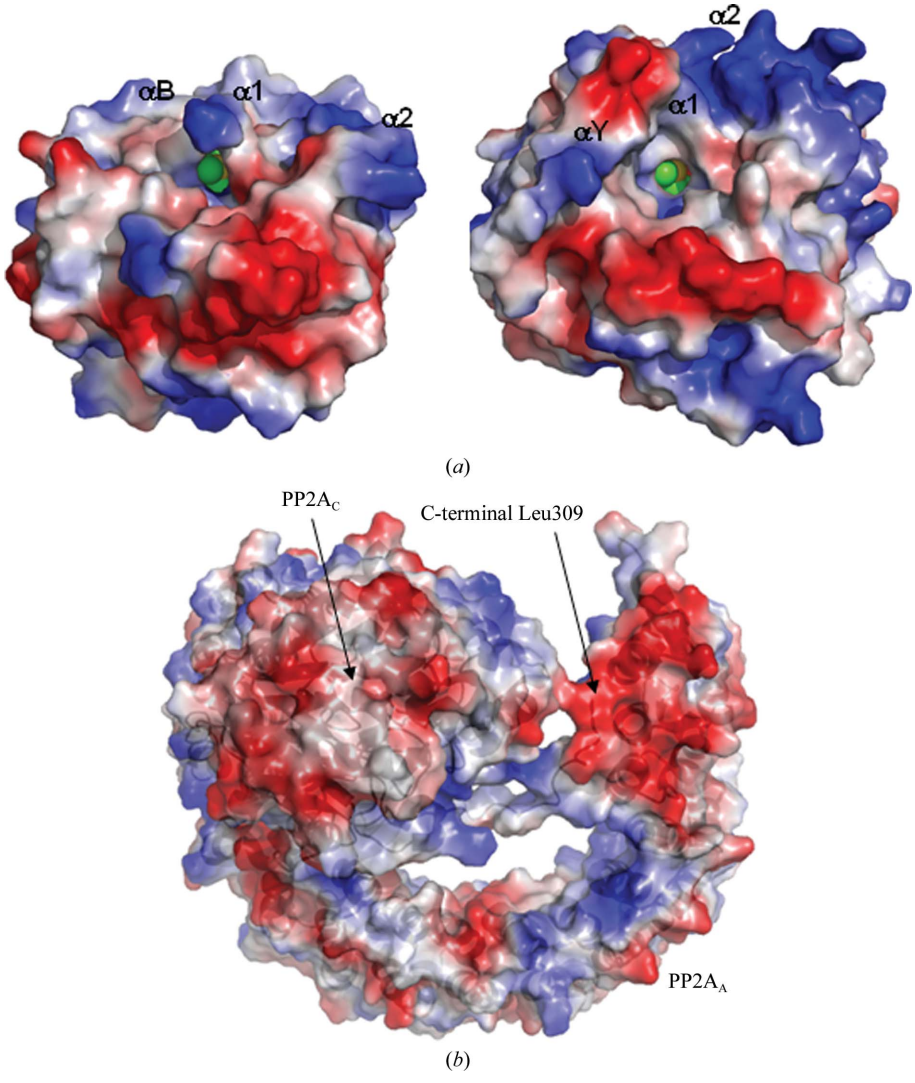


**Figure 5**
Model of the protein–protein interaction with PP2A. (*a*) A qualitative representation of the surface electrostatic potential of LCMT1 was generated using the *PyMOL* viewer (DeLano Scientific). Molecular surfaces of yeast PPM1 (left) and human LCMT1 (right) shown in equivalent orientations reveal narrow grooves providing access to the cofactor. AdoMet is shown in a van der Waals spheres representation, with C, S, O and N atoms coloured green, yellow, red and blue, respectively. In both images an activated methyl group bound to the S atom is visible. Above the active sites in both molecules there are areas of positively charged surface (blue region) suggesting an additional site of association with PP2A. (*b*) Areas of negative surface potential of PP2A$_D$ (red) that might be involved in binding LCMT1. The molecular surface of PP2A$_D$ was made transparent to show ribbon representations of the individual subunits C and A. The position of the C-terminus of the C subunit is indicated.

### 3.5. Putative mode of PP2A interaction with LCMT1

Over the past several years, structures of several proteins that form complexes with PP2A have been determined, including the structures of the holoenzyme with the B′ (PR61; Cho & Xu, 2007; Xu *et al.*, 2006) or B (PR55) subunits (Xu *et al.*, 2008), of SV40 small-T antigen in complex with the PP2A scaffolding subunit (PP2A$_A$; Chen *et al.*, 2007) and of methylesterase PME1 with the PP2A core enzyme (PP2A$_D$; Xing *et al.*, 2008), and these structures can provide some clues regarding the interaction of LCMT1 with PP2A. While B′ (PR61), B (PR55) and SV40 small-T antigen associate with both catalytic PP2A$_C$ and scaffolding PP2A$_A$ subunits, PME1 was only observed to interact with PP2A$_C$. The PP2A$_A$ subunit, which is composed of HEAT repeats, uses different sets of these repeats for intermolecular interactions with various partners, such that HEAT repeats 2, 4 and 5 are involved in the PR61–PP2A$_A$ interaction, whereas HEAT repeats 3–7

are associated with the PR55–PP2A$_A$ interaction. The SV40 small-T antigen, on the other hand, interacts with the intra-HEAT-repeat loops of HEAT repeats 3–7 of the PP2A$_A$ subunit. The association of PP2A$_C$ with various regulatory proteins is even more diverse owing to the different functions that these proteins perform.

Although it is the C-terminal carboxyl group of the PP2A$_C$ subunit that is methylated, the substrate of the LCMT1 enzyme is a PP2A$_D$ core enzyme: a complex between the A and C subunits. Furthermore, LCMT1 does not exhibit any activity towards the synthetic peptide corresponding to the conserved C-terminal motif of PP2A$_C$, suggesting that LCMT1 would also need to recognize other molecular features of PP2A in addition to Leu309. LCMT1 might use protein–protein interactions to orient its active site appropriately towards the C-terminus of PP2A$_C$, which otherwise would be a poor substrate, and this mode of interaction might involve the recognition of specific surfaces on the A subunit or a direct interaction with the C subunit at a site additional to that of the C-terminus, in a fashion similar to that seen for the methylesterase PME1 (Xing *et al.*, 2008). Qualitative examination of the electrostatic surface potential of LCMT1 reveals a positively charged area of the protein (Fig. 5*a*) just above the deep groove leading to the cofactor. This surface is formed by helices $\alpha$2 and $\alpha$B and the flexible loop linking $\alpha$2 to $\alpha$Z of human LCMT1. Examination of the electrostatic surface potential of the core PP2A$_D$ enzyme reveals two complementary negatively charged regions, one on the C subunit and another formed by the C-terminus of PP2A$_C$ and the N-terminal HEAT repeats of the A subunit, suggesting that either of these regions might be involved in protein–protein interaction with LCMT1 (Fig. 5*b*). Preliminary isothermal titration calorimetry experiments with 100 $\mu M$ full-length LCMT1 did not detect any association between LCMT1 and PP2A$_A$ as no significant heat change was observed (data not shown). Thus, we would suggest that either the binding constant for PP2A$_A$ is very low, contrary to what would be expected for the proposed charge–charge surface interaction, or that LCMT1 might only associate with PP2A$_C$. Further verification of this model is needed.

## 4. Conclusions

The crystal structure of the human PP2A leucine carboxyl methyltransferase exhibits strong conservation of the core of the globular structure, including the AdoMet binding site. The unique structural elements representing variation from the common topology are most likely to be involved in protein–protein interactions with its substrate: the catalytic subunit of the key cellular phosphatase PP2A. LCMT1 is involved in the regulation of the methylation-dependent PP2A holoenzyme assembly; however, the full implications of this modification are not well understood. The crystal structure of LCMT1 can be exploited for the development of specific inhibitors serving as molecular tools for investigation of PP2A methylation *in vivo*. The truncated form of the enzyme that we described here is very soluble and crystallized under a diverse range of conditions, providing an excellent platform for the crystallographic study of putative inhibitors.

We thank Dr Gary N. Parkinson (The School of Pharmacy, University of London) for helping us with testing of LCMT1 crystals, Dr Vernon Skinner (SMB/UCL) for mass-spectrometric analysis, Dr Martin Bommer (Birkbeck College) and Dr Andrew Turnbull (CRT/Birkbeck College) for assistance with crystallization and Dr John Christodoulou (SMB/UCL) for critical reading of the manuscript. Professor Jeff Stock at Princeton University provided us with the original partial clone of LCMT1. Initial aspects of this project were funded by a BBSRC UK project grant (B18126).

## References

Alvarado-Kristensson, M. & Andersson, T. (2005). *J. Biol. Chem.* **280**, 6238–6244.
Anderson, N. G., Maller, J. L., Tonks, N. K. & Sturgill, T. W. (1990). *Nature (London)*, **343**, 651–653.
Andjelkovic, N., Zolnierowicz, S., Van Hoof, C., Goris, J. & Hemmings, B. A. (1996). *EMBO J.* **15**, 7156–7167.
Arino, J., Woon, C. W., Brautigan, D. L., Miller, T. B. Jr & Johnson, G. L. (1988). *Proc. Natl Acad. Sci. USA*, **85**, 4252–4256.
Begum, N. & Ragolia, L. (1996). *J. Biol. Chem.* **271**, 31166–31171.
Begum, N. & Ragolia, L. (1999). *Biochem. J.* **344**, 895–901.
Berman, H. M., Westbrook, J., Feng, Z., Gilliland, G., Bhat, T. N., Weissig, H., Shindyalov, I. N. & Bourne, P. E. (2000). *Nucleic Acids Res.* **28**, 235–242.
Bryant, J. C., Westphal, R. S. & Wadzinski, B. E. (1999). *Biochem. J.* **339**, 241–246.
Bryson, K., McGuffin, L. J., Marsden, R. L., Ward, J. J., Sodhi, J. S. & Jones, D. T. (2005). *Nucleic Acids Res.* **33**, W36–W38.
Chatfield, K. & Eastman, A. (2004). *Biochem. Biophys. Res. Commun.* **323**, 1313–1320.
Chen, C.-L., Lin, C.-F., Chiang, C.-W., Jan, M.-S. & Lin, Y.-S. (2006). *Mol. Pharmacol.* **70**, 510–517.
Chen, J., Martin, B. L. & Brautigan, D. L. (1992). *Science*, **257**, 1261–1264.
Chen, J., Parsons, S. & Brautigan, D. L. (1994). *J. Biol. Chem.* **269**, 7957–7962.
Chen, V. B., Arendall, W. B., Headd, J. J., Keedy, D. A., Immormino, R. M., Kapral, G. J., Murray, L. W., Richardson, J. S. & Richardson, D. C. (2010). *Acta Cryst.* D**66**, 12–21.
Chen, Y., Xu, Y., Bao, Q., Xing, Y., Li, Z., Lin, Z., Stock, J. B., Jeffrey, P. D. & Shi, Y. (2007). *Nature Struct. Mol. Biol.* **14**, 527–534.
Chiang, C.-W., Kanies, C., Kim, K. W., Fang, W. B., Parkhurst, C., Xie, M., Henry, T. & Yang, E. (2003). *Mol. Cell. Biol.* **23**, 6350–6362.
Cho, D.-H., Choi, Y. J., Jo, S. A., Ryou, J., Kim, J. Y., Chung, J. & Jo, I. (2006). *Am. J. Physiol. Cell Physiol.* **291**, C317–C326.
Cho, U. S. & Xu, W. (2007). *Nature (London)*, **445**, 53–57.
Collaborative Computational Project, Number 4 (1994). *Acta Cryst.* D**50**, 760–763.
De Baere, I., Derua, R., Janssens, V., Van Hoof, C., Waelkens, E., Merlevede, W. & Goris, J. (1999). *Biochemistry*, **38**, 16539–16547.
Djordjevic, S. & Stock, A. M. (1997). *Structure*, **5**, 545–558.
Emsley, P., Lohkamp, B., Scott, W. G. & Cowtan, K. (2010). *Acta Cryst.* D**66**, 486–501.
Engh, R. A. & Huber, R. (1991). *Acta Cryst.* A**47**, 392–400.
Favre, B., Zolnierowicz, S., Turowski, P. & Hemmings, B. A. (1994). *J. Biol. Chem.* **269**, 16311–16317.
Fontana, A., de Laureto, P. P., Spolaore, B., Frare, E., Picotti, P. & Zambonin, M. (2004). *Acta Biochim. Pol.* **51**, 299–321.
Gabel, S., Benefield, J., Meisinger, J., Petruzzelli, G. J. & Young, M. (1999). *Otolaryngol. Head Neck Surg.* **121**, 463–468.

George, R. R., Harris, R., Nunn, C. M., Cramer, R. & Djordjevic, S. (2002). *Protein Expr. Purif.* **26**, 266–274.
Gomez, N. & Cohen, P. (1991). *Nature (London)*, **353**, 170–173.
Groves, M. R., Hanlon, N., Turowski, P., Hemmings, B. A. & Barford, D. (1999). *Cell*, **96**, 99–110.
Guo, C. Y., Brautigan, D. L. & Larner, J. M. (2002). *J. Biol. Chem.* **277**, 4839–4844.
Hemmings, B. A., Adams-Pearson, C., Maurer, F., Müller, P., Goris, J., Merlevede, W., Hofsteenge, J. & Stone, S. R. (1990). *Biochemistry*, **29**, 3166–3173.
Janssens, V. & Goris, J. (2001). *Biochem. J.* **353**, 417–439.
Janssens, V., Goris, J. & Van Hoof, C. (2005). *Curr. Opin. Genet. Dev.* **15**, 34–41.
Jordens, J., Janssens, V., Longin, S., Stevens, I., Martens, E., Bultynck, G., Engelborghs, Y., Lescrinier, E., Waelkens, E., Goris, J. & Van Hoof, C. (2006). *J. Biol. Chem.* **281**, 6349–6357.
Karaiskou, A., Jessus, C., Brassac, T. & Ozon, R. (1999). *J. Cell Sci.* **112**, 3747–3756.
Larkin, M. A., Blackshields, G., Brown, N. P., Chenna, R., McGettigan, P. A., McWilliam, H., Valentin, F., Wallace, I. M., Wilm, A., Lopez, R., Thompson, J. D., Gibson, T. J. & Higgins, D. G. (2007). *Bioinformatics*, **23**, 2947–2948.
Laskowski, R. A., MacArthur, M. W., Moss, D. S. & Thornton, J. M. (1993). *J. Appl. Cryst.* **26**, 283–291.
Lechward, K., Awotunde, O. S., Swiatek, W. & Muszynska, G. (2001). *Acta Biochim. Pol.* **48**, 921–933.
Lee, J. & Stock, J. (1993). *J. Biol. Chem.* **268**, 19192–19195.
Lee, T. H. (1995). *Semin. Cancer Biol.* **6**, 203–209.
Leulliot, N., Quevillon-Cheruel, S., Sorel, I., de La Sierra-Gallay, I. L., Collinet, B., Graille, M., Blondeau, K., Bettache, N., Poupon, A., Janin, J. & van Tilbeurgh, H. (2004). *J. Biol. Chem.* **279**, 8351–8358.
Liauw, S. & Steinberg, R. A. (1996). *J. Biol. Chem.* **271**, 258–263.
Lin, X.-H., Walter, J., Scheidtmann, K., Ohst, K., Newport, J. & Walter, G. (1998). *Proc. Natl Acad. Sci. USA*, **95**, 14693–14698.
Longin, S., Jordens, J., Martens, E., Stevens, I., Janssens, V., Rondelez, E., De Baere, I., Derua, R., Waelkens, E., Goris, J. & Van Hoof, C. (2004). *Biochem. J.* **380**, 111–119.
Longin, S., Zwaenepoel, K., Louis, J. V., Dilworth, S., Goris, J. & Janssens, V. (2007). *J. Biol. Chem.* **282**, 26971–26980.
Martin, J. L. & McMillan, F. M. (2002). *Curr. Opin. Struct. Biol.* **12**, 783–793.
McCoy, A. J., Grosse-Kunstleve, R. W., Adams, P. D., Winn, M. D., Storoni, L. C. & Read, R. J. (2007). *J. Appl. Cryst.* **40**, 658–674.
Millward, T. A., Zolnierowicz, S. & Hemmings, B. A. (1999). *Trends Biochem. Sci.* **24**, 186–191.
Murshudov, G. N., Vagin, A. A. & Dodson, E. J. (1997). *Acta Cryst.* D**53**, 240–255.
Ogris, E., Du, X., Nelson, K. C., Mak, E. K., Yu, X. X., Lane, W. S. & Pallas, D. C. (1999). *J. Biol. Chem.* **274**, 14382–14391.
Perdiguero, E. & Nebreda, A. R. (2004). *Cell Cycle*, **3**, 733–737.
Pflugrath, J. W. (1999). *Acta Cryst.* D**55**, 1718–1725.
Schonthal, A. H. (2001). *Cancer Lett.* **170**, 1–13.
Schubert, H. L., Blumenthal, R. M. & Cheng, X. (2003). *Trends Biochem. Sci.* **28**, 329–335.
Sontag, E., Nunbhakdi-Craig, V., Sontag, J. M., Diaz-Arrastia, R., Ogris, E., Dayal, S., Lentz, S. R., Arning, E. & Bottiglieri, T. (2007). *J. Neurosci.* **27**, 2751–2759.
Srinivasan, M. & Begum, N. (1994). *J. Biol. Chem.* **269**, 12514–12520.
Stone, S. R., Hofsteenge, J. & Hemmings, B. A. (1987). *Biochemistry*, **26**, 7215–7220.
Tanimukai, H., Grundke-Iqbal, I. & Iqbal, K. (2005). *Am. J. Pathol.* **166**, 1761–1771.
Tian, Q. & Wang, J. (2002). *Neurosignals*, **11**, 262–269.
Tsujio, I., Zaidi, T., Xu, J., Kotula, L., Grundke-Iqbal, I. & Iqbal, K. (2005). *FEBS Lett.* **579**, 363–372.
Vagin, A. & Teplyakov, A. (2010). *Acta Cryst.* D**66**, 22–25.
Van Hoof, C. & Goris, J. (2004). *Cancer Cell*, **5**, 105–106.
Wang, Y. & Ng, T.-Y. (2006). *Mol. Biol. Cell*, **17**, 80–89.
Wu, J., Tolstykh, T., Lee, J., Boyd, K., Stock, J. B. & Broach, J. R. (2000). *EMBO J.* **19**, 5672–5681.
Xie, H. & Clarke, S. (1993). *J. Biol. Chem.* **268**, 13364–13371.
Xin, M. & Deng, X. (2006). *J. Biol. Chem.* **281**, 18859–18867.
Xing, Y., Li, Z., Chen, Y., Stock, J. B., Jeffrey, P. D. & Shi, Y. (2008). *Cell*, **133**, 154–163.
Xu, Y., Chen, Y., Zhang, P., Jeffrey, P. D. & Shi, Y. (2008). *Mol. Cell*, **31**, 873–885.
Xu, Y., Xing, Y., Chen, Y., Chao, Y., Lin, Z., Fan, E., Yu, J. W., Strack, S., Jeffrey, P. D. & Shi, Y. (2006). *Cell*, **127**, 1239–1251.
Yan, Z., Fedorov, S. A., Mumby, M. C. & Williams, R. S. (2000). *Mol. Cell. Biol.* **20**, 1021–1029.
Zhang, C.-E., Tian, Q., Wei, W., Peng, J.-H., Liu, G.-P., Zhou, X.-W., Wang, Q., Wang, D.-W. & Wang, J.-Z. (2008). *Neurobiol. Aging*, **29**, 1654–1665.
Zhu, T., Matsuzawa, S., Mizuno, Y., Kamibayashi, C., Mumby, M. C., Andjelkovic, N., Hemmings, B. A., Onoe, K. & Kikuchi, K. (1997). *Arch. Biochem. Biophys.* **339**, 210–217.
Zolnierowicz, S. (2000). *Biochem. Pharmacol.* **60**, 1225–1235.